Oblique Shock Formation in Impulsively Started Wedge Flows

J. Falcovitz*
Technion—Israel Institute of Technology, Haifa 32000, Israel
Y. Kivity†
Rafael Ballistic Center, Haifa, Israel
and
D. Weihs‡
Technion—Israel Institute of Technology, Haifa 32000, Israel

Introduction

In stationary supersonic flow over a sharp wedge of half-angle δ, an oblique shock is attached to the leading edge, deflecting the flow velocity into an orientation parallel to the wedge surface (Sec. 117 of Ref. 1), provided $\delta < \delta_{max}$ where δ_{max} is a function of the oncoming flow Mach number M_1.

Recently, Weihs and Freitas[2] presented an approximate model for the rate of formation of the oblique shock. In their model, the endpoint of the steadily growing oblique shock front was envisioned as sliding in the stationary oblique shock direction. The sliding speed was governed by acoustic perturbations emanating from the wedge vertex and propagating in the uniform flow state corresponding to a stationary oblique shock. Their solution (designated herein as WF) indicated that the shock formation speed is always somewhat higher than the incoming undisturbed velocity, i.e., $(M_f/M_1) > 1$. This ratio was shown to be a function of the wedge angle δ, the ratio of specific heats γ (assuming a perfect gas) and M_1.

Further examination of the shock formation process leads to the conclusion that a more accurate model can be devised, still in the realm of simple analysis.

The self-similar impulsively started flow near a wedge of finite half-angle was described qualitatively by Sakurai.[3] He pointed out that when the flow commences abruptly (either by setting the fluid in motion or by impulsive acceleration of the wedge), the self-similar shock formed about the wedge consists of three segments (Fig. 1): 1) a plane oblique shock attached to the leading edge, having uniform intensity; 2) a curved transient shock of nonuniform intensity; and 3) a plane uniform stopping shock parallel to the wedge surface.

In regions 1 and 3 the flow is uniform, and in region 2 it is nonuniform. No solutions exist for this nonuniform region.

The present study formulates an alternative, more accurate model for the rate of formation of the oblique shock. The accuracy of the model is checked by comparison with numerical computations, which, in the absence of experimental data, are our sole guideline.

Shock Formation Model

The effect of the wedge surface very far from the leading edge is to deflect the oncoming flow so that its velocity vector becomes parallel to the wedge surface. This deflection is done by a stopping shock (*BW* in Fig. 1) parallel to the wedge surface, whose intensity corresponds to the effective "piston speed" $U_1 \sin\delta$, where U_1 is the oncoming flow speed. The velocity at the uniform post-shock state $(\ )_n$ is $U_1 \cos\delta$, parallel to the wedge surface. The sound speed C_n and the velocity of propagation of the shock relative to the wedge V_n are derived from standard normal shock expressions (Secs. 67, 68 of Ref. 1) as follows:

$$M_n = \left(\frac{\gamma+1}{4}\right) M_1 \sin\delta + \left[1 + \left(\frac{\gamma+1}{4} M_1 \sin\delta\right)^2\right]^{1/2} \tag{1a}$$

$$V_n = (M_n - M_1 \sin\delta) C_1 \tag{1b}$$

$$\frac{C_n}{C_1} = (\gamma+1)^{-1}[2(\gamma-1)]^{1/2} M_n^{-1} \left(1 + \frac{\gamma-1}{2} M_n^2\right)^{1/2} \times \left(\frac{2\gamma}{\gamma-1} M_n^2 - 1\right)^{1/2} \tag{1c}$$

The formation of the transition region (*QB* in Fig. 1) is envisioned as follows. Point *P* denotes the location of the "first fluid particle" that moves along the wedge surface from its leading edge at the speed corresponding to the uniform state $(\ )_n$, i.e., $U_1 \cos\delta$. The perturbations caused by the leading edge are deemed emanating from point *P* at the sound speed C_n relative to the fluid in state $(\ )_n$. Hence, by considering the wave-front diagram presented in Fig. 1, the location of the shock-formation endpoint *B* is given by

$$(OB)^2 = (OP)^2 + (PB)^2 + 2(OP)(PB)\cos\theta \tag{2}$$

where

$$(OP) = U_1 t \cos\delta;\ (PB) = C_n t;\ \sin\theta = \frac{V_n}{C_n}$$

Obviously, Eq. (2) is valid only if $(V_n/C_n) < 1$, which implies in terms of the wave diagram that the perturbations emanating from point *P* would always catch up with the stopping shock. Since the velocity of the fluid at state $(\ )_n$ is parallel to the wedge surface, the stopping shock speed V_n is also its speed relative to the fluid at the post-shock state. Hence the condition $V_n < C_n$ holds by virtue of the stipulation that a normal shock always propagates at subsonic speed relative to the post-shock fluid (Sec. 65 of Ref. 1). The speed of formation, expressed as a Mach number M_B (normalized by C_1) is readily obtained from Eq. (2) as

$$\frac{V_B}{C_1} = M_B = [M_1^2 \cos^2\delta + (C_n/C_1)^2 + 2M_1(C_n/C_1)\cos\delta\cos\theta]^{1/2} \tag{3}$$

Rate of Formation Results

The numerical computations were performed with the commercially available PISCES code.[4] The numerical scheme employed by this code is a second-order extension to the Godunov[5] scheme. The hydrodynamic laws for conservation

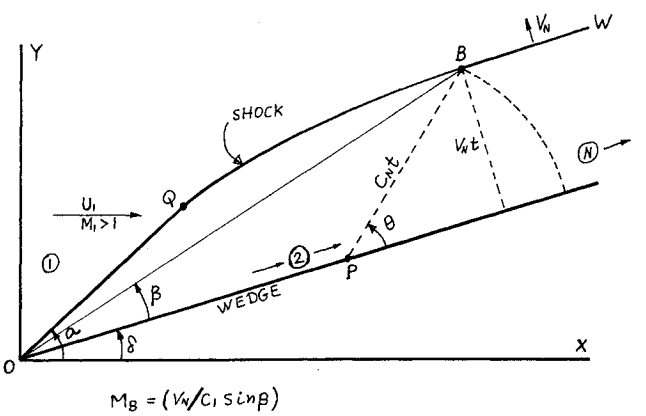

Fig. 1 Shock formation in an impulsively started wedge flow. *OQ* is the planar oblique shock, *QB* is a curved transition shock, and *BW* is the planar stopping shock (parallel to wedge surface).

Received March 17, 1992; revision received July 24, 1992; accepted for publication July 27, 1992.

*Associate Professor, Department of Aerospace Engineering. Member AIAA.
†Research Fellow, P.O. Box 2250.
‡Professor, Department of Aerospace Engineering.

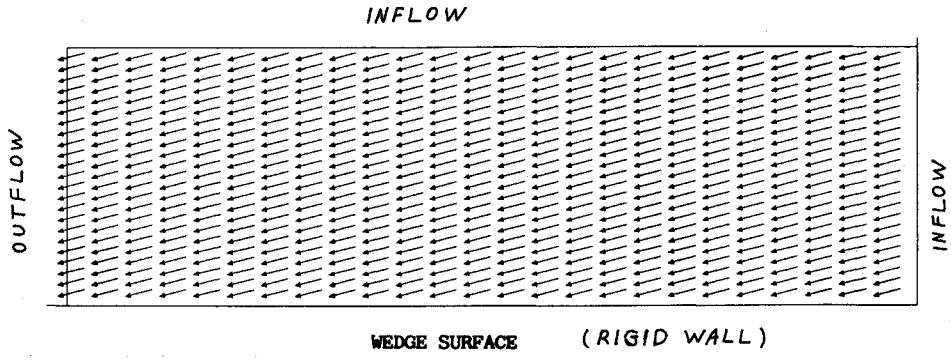

Fig. 2a Computational scheme for the numerical evaluation of shock formation; $\delta = 0.25$, $M_1 = 3$.

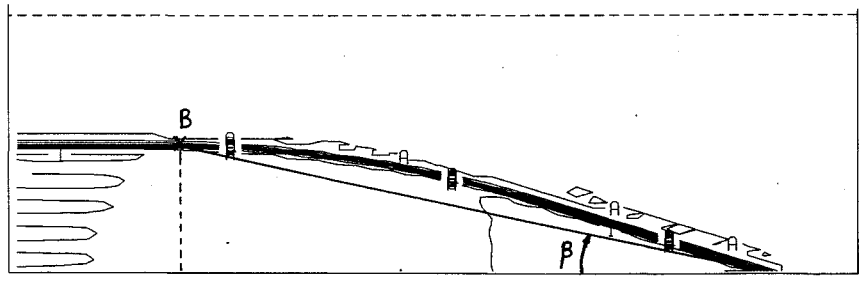

Fig. 2b Isobars indicating the captured shock front.

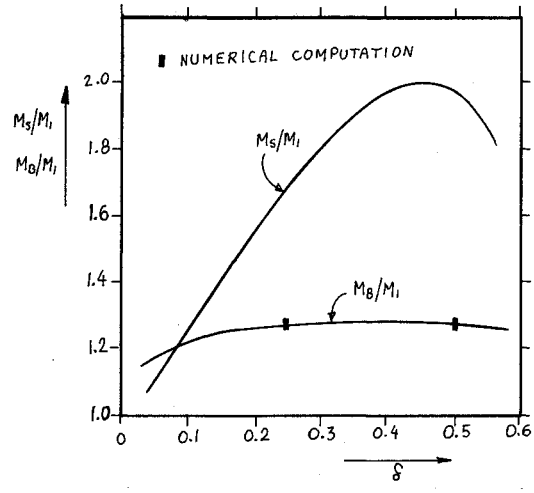

Fig. 3 Rate of shock formation as function of wedge half-angle δ, at flow Mach number $M_1 = 3$. M_S is obtained from WF[2], M_B is from the present model [Eq. (2)]. Curves end when $\delta = \delta_{max}$.

of mass, momentum, and energy are time-integrated at rectangular cells using fluxes (obtained from solving the local Riemann problem) that resolve the jump between adjacent cells at each cell interface. The scheme of the computational grid is depicted in Fig. 2 along with the results of a sample computation in the form of isobars marking the shock front. Point B is read by inspection from the curve, and we estimate the accuracy of M_B thus determined at $\pm 1\%$. This accuracy level estimate is obtained as follows.

Shock fronts obtained from such computations are typically smeared over about one element and are thus determined by inspecting an isobars plot for a strip of steepest normal pressure gradient. The present computation (Fig. 2) was performed on a grid of 23×25 elements. Convergence was verified by repeating the computation using double- and quadruple-density grids (in each direction), and demonstrating that shock fronts did not change appreciably. An additional check, which was possible in the present particular case of impulsively started supersonic flow, is to check the oblique shock angle (corresponding to OQ in Fig. 1) and the distance $V_n t$ through which the normal shock has propagated at time t (segment BW in Fig. 1). Both agreed very well with the corresponding analytic value. This agreement led us to estimate the accuracy of determining the shock front from an isobars plot at $\pm 1\%$. Since the Mach number M_B is related to the location of point B (Fig. 1) by $M_B = V_n/C_1 \sin\beta$, the only parameter that had to be determined from the isobars plot (Fig. 2) was β. By inspecting double- and even higher-density computations, we estimated the accuracy of determining β (and hence M_B) also at about $\pm 1\%$. This level of accuracy is symbolically reflected by the vertical bars depicting computational points in Fig. 3. Certainly the accuracy of determining these points far exceeds the discrepancy between the present and the WF[2] models for the rate of formation of the oblique shock.

Shock formation rates predicted by the present model are presented in Fig. 3, along with the predictions of the previous WF model[2] denoted as M_S/M_1 and the two points obtained from numerical computations. The good agreement of the present model with numerically computed formation rates clearly shows that it is more accurate than the WF model. It is also of interest to note that the rate of formation M_B is nearly constant for all δ, in spite of the strongly nonlinear expression (3) for M_B. As in the WF model, a maximum in M_B/M_1 is obtained (Fig. 3). However, in the present model the maximum is not nearly as pronounced as in the WF model, and its location is at a value of wedge angle δ that is not near the maximum deflection angle for attached oblique shock δ_{max}. Indeed, the present model is valid even for $\delta > \delta_{max}$ since it is not contingent on the existence of an attached oblique shock. In this case, however, the shock formation would take up a different pattern (just two zones instead of three), and we do not consider it within the framework of the present model.

Concluding Remarks

The present model is in considerably better agreement with numerically computed shock-formation rates than the former one (WF). It seems that the crucial element missing in WF is the incorporation of the curved transition segment of the forming shock into the model. It turns out, as demonstrated by the manner in which the present model was formulated, that the transition segment can be accounted for approximately without explicitly resorting to curved shock analysis.

This approximation was done by considering solely the endpoint of the curved shock (point B in Fig. 3), which also denotes the beginning of the normal stopping shock.

References

[1]Courant, R., and Friedrichs, K. O., *Supersonic Flow and Shock Waves,* Interscience, New York, 1948.

[2]Weihs, D., and Freitas, C. J., "Rate of Formation of Oblique Shock Waves," *AIAA Journal,* Vol. 29, No. 8, 1991, pp. 1342-1344.

[3]Sakurai, A., "The Flow Due to Impulsive Motion of a Wedge and Its Similarity to the Diffraction of Shock Waves," *Journal of the Physical Society of Japan,* Vol. 10, No. 3, 1955, pp. 221-228.

[4]Hancock, S. L., *PISCES 2DELK Theoretical Manual,* Physics International, San Leandro, CA, Aug. 1985.

[5]Godunov, S. K., "A Finite Difference Method for the Numerical Computation and Discontinuous Solutions of the Equations of Fluid Dynamics," Mat. Sbornik, Vol. 47, 1959, pp. 271-295.

Experimental Investigations of Asymmetric Vortex Flows Behind Elliptic Cones at Incidence

Wolfgang H. Stahl*

King Fahd University of Petroleum and Minerals, Dhahran 31261, Saudi Arabia

I. Introduction

In a recent investigation, the low-speed flow past a slender, circular cone at high incidence was studied with respect to leeside vortex-flow asymmetry and its suppression by means of a fin between the vortices.[1] The use of such a fin proved to be effective in establishing, at least nominally, symmetric vortex-flow configurations. It was reported in fairly early work[2] and more recently in Ref. 3, that on slender delta wings in low-speed flow the initially symmetric leading-edge vortices on the leeside became asymmetric at some critical incidence. Therefore, the application of a fin was also considered for suppressing asymmetric vortex flow on slender delta wings. To this end, flow observations were carried out on two slender, sharp-edged delta wings of different aspect ratios A in a water tunnel at high incidence; they revealed that the vortex flow remained symmetric in the incidence range investigated. This result was confirmed in low-speed wind-tunnel tests at a larger Reynolds number. Reported strong vortex-flow asymmetry on a slender delta wing is possibly related to the probably more or less thick, elliptic-cone shape of the tip.[4,5] These findings have recently been confirmed by results reported in Ref. 6.

It is assumed that the flow past a sharp-edged delta wing at incidence, particularly the leeside vortex flow, is representative of the flow past a very thin, flat, delta plate (thickness ratio $\tau = t/b \to 0$, where t = thickness and b = span); such a very thin, flat, delta plate represents a very thin elliptic cone ($\tau \to 0$). One could then surmise that there should be some intermediate cone with a certain finite thickness between the thin, flate-plate delta and the thick, circular cone, for which the flow changes from symmetric to asymmetric at a given incidence.

Some light was shed on the development of the vortex configurations on bodies of different relative thicknesses at a given incidence in recent theoretical work by Fiddes and Williams.[7] They presented results of an inviscid-flow study of vortex-flow asymmetry on slender bodies of various cross sections. The separating flow was represented by a vortex-sheet model, and the particular form used was that of Smith.[8] Together with the results obtained by Smith[9] for the separation of a vortex sheet from a smooth surface, Fiddes[10] developed a vortex-sheet model for inviscid flow past slender circular and elliptic cones at incidence. In this inviscid-flow model separation-line positions were specified as a parameter. Solutions were obtained for the flow with symmetric separation-line positions prescribed. Two families of solutions occurred: one for symmetric and one for strongly asymmetric vortex flow.

In Ref. 7, results are reported on the effect of thickness ratio of elliptic cones on vortex-flow asymmetry: The degree of asymmetry is reduced as the thickness ratio is decreased, and at 52% thickness the asymmetry has vanished at the specific incidence chosen. At higher incidences, the thickness ratio needed to suppress asymmetry decreases. These results suggest that on thin elliptic cones, and in the limit on delta plates, vortex-flow asymmetry may not be found. This was confirmed by results when using a simpler line-vortex model.[7]

It was considered to be of interest to check experimentally our earlier-mentioned conclusions and the results of the preceding theory as to the dependence of degree of vortex-flow asymmetry on the cones' thickness ratio. To this end, three elliptic cones of thickness ratios $\tau = 1.0$, 0.65, and 0.40, respectively, as well as a sharp-edged delta wing, with τ varying between 0.09 and 0.18 along the chord, were studied in a water tunnel at high incidence by using a dye flow-visualization technique.

II. Models, Testing Facility, and Flow-Visualization Technique

The models investigated are depicted in Fig. 1. Each model was supported by a thin rod, extending to the rear; the rod, in turn, was fixed at its rear end to a vertical strut system. The water tunnel of

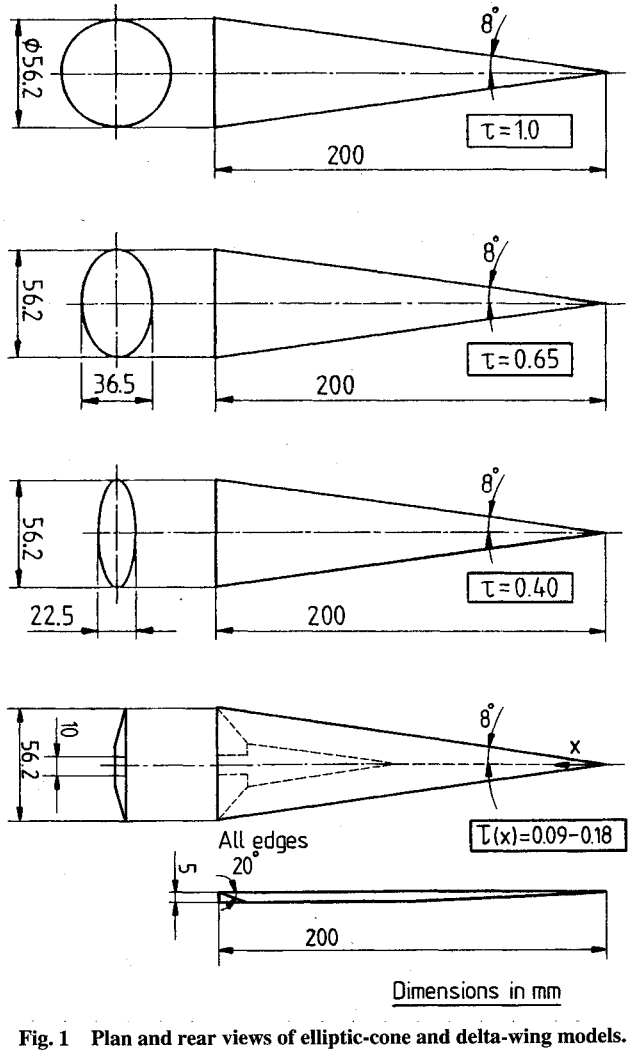

Fig. 1 Plan and rear views of elliptic-cone and delta-wing models.

Received Feb. 27, 1992; revision received Aug. 17, 1992; accepted for publication Sept. 21, 1992.

*Adjunct Professor, Department of Mechanical Engineering; currently, Visiting Scientist, DLR, Göttingen, Germany. Senior Member AIAA.